DRAFT
SAND2017-1286C
Proceedings of the 11th International Conference on Energy Sustainability
ES2017
June 26 – June 30, 2017, Charlotte, North Carolina, USA

PowerEnergy2017-3524

Design and Testing of a Novel Bladed Receiver

Jesus D. Ortega
Sandia National Laboratories, Concentrating Solar Technologies Department
Albuquerque, NM 87185-1127, USA.

Joshua M. Christian
Sandia National Laboratories, Concentrating Solar Technologies Department
Albuquerque, NM 87185-1127, USA.

Clifford K. Ho
Sandia National Laboratories, Concentrating Solar Technologies Department
Albuquerque, NM 87185-1127, USA.

ABSTRACT

Previous research at Sandia National Laboratories showed the potential advantages of using light-trapping features which are not currently used in direct tubular receivers. A horizontal bladed receiver arrangement showed the best potential for increasing the effective solar absorptance by increasing the ratio of effective surface area to the aperture footprint. Ray-tracing analyses using SolTrace were performed to understand the light-trapping effects of the bladed receivers, which enable re-reflections between the fins that enhance the effective solar absorptance. A parametric optimization study was performed to determine the best possible configuration with a fixed intrinsic absorptivity of 0.9 and exposed surface area of 1 m^2. The resulting design consisted of three vertical panels 0.584 m long and 0.508 m wide and 3 blades 0.508 m long and 0.229 m wide with a downward tilt of 50 degrees from the horizontal. Each blade consisted of two panels which were placed in front of the three vertical panels. The receiver was tested at the National Solar Thermal Test Facility using pressurized air. However, the receiver was designed to operate using supercritical carbon dioxide (sCO_2) at 650 °C and 15 MPa for 100,000 hours following the *ASME Boiler and Pressure Vessel Code Section VIII Division 1*. The air flowed through the leading panel of the blade first, and then recirculated toward the back panel of the blade before flowing through one of the vertical back panels. The test results of the bladed receiver design showed a receiver efficiency increase over a flat receiver panel of ~5 - 7% (from ~80% to ~86%) over a range of average irradiances, while showing that the receiver tubes can withstand temperatures > 800 °C with no issues. Computational fluid dynamics (CFD) modeling using the Discrete Ordinates (DO) radiation model was used to predict the temperature distribution and the resulting receiver efficiencies. The predicted thermal efficiency and surface temperature values correspond to the measured efficiencies and surface temperatures within one standard deviation. In the near future, an sCO_2 flow system will be built to expose the receiver to higher pressure and fluid temperatures which could yield higher efficiencies.

1. INTRODUCTION

Direct tubular receivers configured externally for central power towers have been extensively studied in simulations and pilot-plant experiments. Solar One and Solar Two pilot-plant projects are prime examples of external cylindrical receiver designs. The Solar Two receiver efficiency was proven to reach up to 88% [1] on multiple occasions. These types of receivers are comprised of multiple panels, which in turn are composed of many straight tubes which transfer the heat to the fluid. Novel advances in receiver design must be achieved in order to achieve the current goal from the SunShot initiative which requires a receiver efficiency > 90% [2].

An analysis report by Rocketdyne evaluated some star receiver geometry concepts [3]. The findings in this report showed that although there were some advantages in the star receiver geometries, there were more complications in the engineering design compared to a conventional cylindrical receiver. Nonetheless, the potential thermal efficiency advantages of these receivers were not fully evaluated. This work led to new research at Sandia National Laboratories

Sandia National Laboratories is a multi-mission laboratory managed and operated by Sandia Corporation, a wholly owned subsidiary of Lockheed Martin Corporation, for the U.S. Department of Energy's National Nuclear Security Administration under contract DE-AC04-94AL85000

showing the potential advantages of using light-trapping novel features which are not currently used in direct tubular receivers as shown in Figure 1 [4]. Christian et al. recently showed that by manipulating the receiver geometries, the thermal efficiency can increase by reducing radiative heat loss from the system [5]. This study showed that the receiver solar absorptivity was very impactful on design choices.

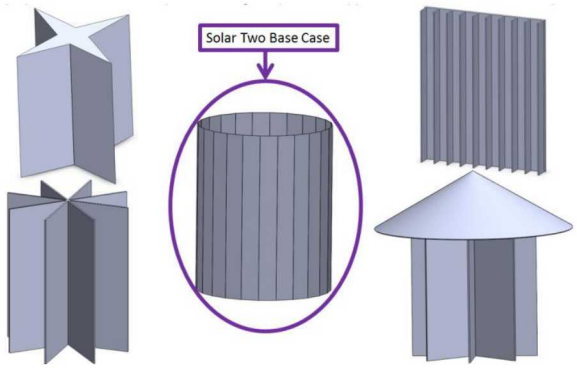

Figure 1.Initial receiver design for comparison to a base-case cylindrical receiver [4].

In conventional cylindrical receiver designs, most of the reflected and thermally emitted radiation is lost to the environment resulting in a due to the receiver view factors close to 1. If the receiver panels can be arranged in a way to lower the external view factors, some of the reflected and thermally emitted radiation can be "re-captured" by the panels; hence the solar absorptivity is increased. A horizontal bladed receiver arrangement showed the best potential for increasing the effective solar absorptance by increasing the ratio of effective surface area to the aperture footprint [5]. Sandia is has built and tested a prototype receiver which was compared to a flat panel receiver.

As shown in Figure 2, the bladed receiver has many options in terms of number of fins, number of tubes, and the angle of the fins (with respect to the vertical). The design, modeling and experimental results of a tubular bladed receiver as discussed by Christian et al. [5] will be discussed in this paper.

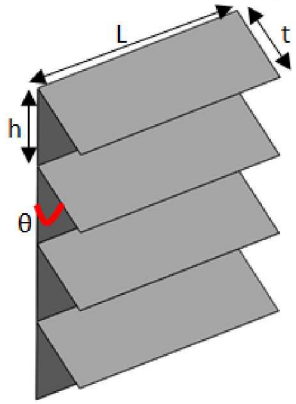

Figure 2.Bladed receiver dimensions based on effective solar absorptance.

The three technical objectives that served as a guideline for developing the bladed receiver for testing were [5]:

1. Increase the light trapping and effective solar absorptance of the receiver.
2. Reduce the thermal emittance of the receiver by taking advantage of local view factors in the hottest regions of the receiver.
3. Increase the thermal efficiency of the receiver by increasing concentration ratio of the receiver through the use of a smaller overall aperture size (optical intercept) while maintaining the same exposed surface area and power.

2. PANEL DESIGN AND FABRICATION

The design of the bladed receiver followed the requirements specified for a pressure vessel in the *American Society of Mechanical Engineer Boiler and Pressure Vessel Code* (*ASME BPVC*).

The following design conditions were taken from the SunShot initiative [3] requirements:

- Design Pressure: 20MPa
- Design Temperature: 700°C
- Design Life: 100,000 hours of operation

As suggested by Ortega et al. [6] Inconel 625 was selected for this analysis, since the allowable stresses for the desired operating temperature are comparable to that of Haynes 230 or Inconel 617, but the availability of Inconel 625 makes it very suitable for solar applications.

In a similar study, Ortega et al. [7] show that the three main drawbacks of using the code exclusively and without any modifications inclined to CSP applications are:

1. Although *Section I* considers the design of power boilers and super-heaters, it is mainly design for power plants which typically are convectively heated by flue gas at relatively low rates of thermal flux [8].

2. The large safety requirements developed for nuclear components in *Section III, Division I – Subsection NH* will require further simplifications since the level of conservatism in the creep-fatigue analyses is not necessary for CSP applications [8].

3. *Section VIII-Division 1* does not consider high-cycle fatigue [8] and therefore the Design-by-Rule methodology does not capture the complete analysis required for solar thermal receivers.

Section VIII was selected to be the most applicable since it considers higher operating temperatures and stress levels even though it does not require detailed calculations. Although it is

known that the safety factors considered in the Section VIII might not be necessarily applicable to solar applications, it has lower safety factors than those in *Section I* (Boilers) and *Section III* (Nuclear Vessels) [7]. A Sandia National Laboratories SAND report contains all the relevant details for the procedure to use *Section VIII* [9].

2.1. Panel design

The number of tubes per panel was determined from the optical modeling studies [5]. These panels had a nominal size and configuration. The receiver configuration selected requires the back panels to have 13 tubes and the fins to have 18 tubes. In order to try and exploit the technical objective 2, the fins will be separated into two panels to explore the influence in localized "hot regions" throughout the receiver. Figure 3 shows the configurations of the two different panels were designed with the least differences.

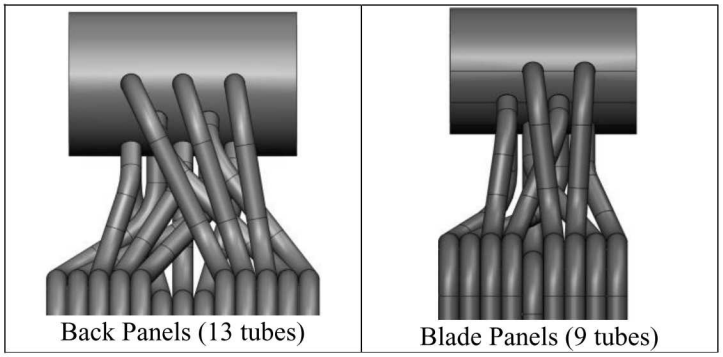

Figure 3.The manifolds were designed to accommodate the number of tubes for each panel.

Knowing the size requirements, the minimum wall thickness required and maximum allowable working pressures were determined using the UG-27 and UG-34 equation [8]. Table 1Table 4 show the results of the design calculations based on the sizes available in stock commercially.

Table 1.Minimum header pipe thicknesses and maximum allowable working pressure calculated by UG-27 at design conditions [9].

3" sch80 pipe (Header)		
PIPE OD	88.9	mm
PIPE WALL	7.62	mm
INSIDE RADIUS	36.83	mm
DESIGN PRESSURE	15	MPa
EFFICIENCY (UG-53)	0.6	
CORROSION ALLOWANCE	-	mm
MANUFACTURING TOLERANCE	0.127	mm
DESIGN TEMPERATURE	650	°C
ALLOWABLE STRESS	137.9	MPa
MINIMUM THICKNESS	7.62	mm
MAXIMUM ALLOWABLE WORKING PRESSURE	15.2	MPa

Table 2.Minimum tube thicknesses and maximum allowable working pressure calculated by UG-27 at design conditions [9].

1/2" Tube		
PIPE OD	12.7	mm
PIPE WALL	1.651	mm
INSIDE RADIUS	4.699	mm
DESIGN PRESSURE	15	MPa
EFFICIENCY (UG-53)	1.0	
CORROSION ALLOWANCE	-	mm
MANUFACTURING TOLERANCE	0.127	mm
DESIGN TEMPERATURE	650	°C
ALLOWABLE STRESS	137.9	MPa
MINIMUM THICKNESS	0.67	mm
MAXIMUM ALLOWABLE WORKING PRESSURE	40.02	MPa

Table 3.Minimum inlet/outlet pipe thicknesses and maximum allowable working pressure calculated by UG-27 at design conditions [9].

3/4" sch40 pipe (Inlet/Outlet Pipe)		
PIPE OD	26.67	mm
PIPE WALL	2.87	mm
INSIDE RADIUS	10.465	mm
DESIGN PRESSURE	15	MPa
DICTICATING EFFICIENCY UG-53	1.0	
CORROSION ALLOWANCE	-	mm
MANUFACTURING TOLERANCE	0.127	mm
DESIGN TEMPERATURE	650	°C
ALLOWABLE STRESS	137.9	MPa
MINIMUM THICKNESS	1.34	mm
MAXIMUM ALLOWABLE WORKING PRESSURE	32.48	MPa

Table 4.Minimum header cap thicknesses and maximum allowable working pressure calculated by UG-27 and UG-34 at design conditions [9].

¾" End Caps		
PIPE OD	88.9	mm
PIPE WALL	7.62	mm
INSIDE RADIUS	36.83	mm
DESIGN PRESSURE	15	MPa
DICTICATING EFFICIENCY UG-53	0.85	
CORROSION ALLOWANCE	-	mm
MANUFACTURING TOLERANCE	0.127	mm

ATTACHEMENT COEFFICIENT	0.3	
DESIGN TEMPERATURE	650	°C
ALLOWABLE STRESS	137.9	MPa
MINIMUM THICKNESS	14.56	mm
PLATE THICKNESS	19.05	mm
MAXIMUM ALLOWABLE WORKING PRESSURE	104.53	MPa

The pre-established design conditions had to be modified. The maximum allowable working pressure was reduced from 20 MPa to 15 MPa while the maximum operating temperature was reduced from 700°C to 650°C. The header pipe was the limiting element in the assembly due to the required thickness. For 3" pipes, typically schedules 40 and 80 are stocked and schedule 160 would require a mill scale production order.

2.2. Panel manufacturing

The weld design requirements for the area of reinforcement can be found in UG-37 while the weld strength analysis is located in UG-41 of *Section VIII* [8].

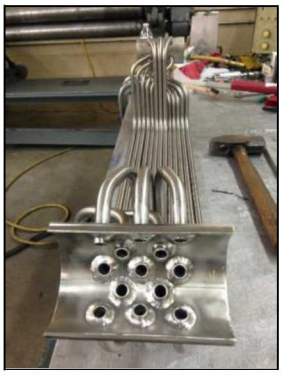

(a) 3 mm internal welds of all components

(b) Completed panels

(c) The full-penetration weld was performed under a Helium atmosphere.

(d) The full penetration can be observed in the circled areas on the header

Figure 4.Construction and welding of the tubular panels.

The area of reinforcement of the tubes penetrating the header pipe, shown in Figure 4a, is calculated using the methodology shown in UG-37. In all instances, the area available is larger than the area required which means no further reinforcement is required other than the internal fillet welds. The header pipes were cut into two longitudinal halves to perform the tube welds internally. This procedure does not affect the performance of the headers since the efficiency is already 60% as shown in Table 1. The efficiency will remain the same as long as the seam weld, to join the halves, is fully penetrating as per UW-12 requirements [8]. J-grooves allow for a best full-penetration as shown in Figure 4d.

The manufacturing of the Inconel 625 panels had to be done by a certified machine shop since it is considered a pressure vessel. The certification was completed by *ASME BPVC Section VIII* Standards.

3. FLAT AND BLADED RECEIVER MODELING

The equations describing mass, momentum and energy transport, and the two equation SST (Shear Stress Transport) k-ω turbulence model were solved using ANSYS Fluent 16. The steady state, pressure based solver using SIMPLE algorithm and second-order upwind for spatial discretization was used for the simulation. Mass flux, energy flux and scaled residuals were continuously monitored as the solution developed, and convergence was assumed only when the quantities of interest exhibited negligible variation.

3.1. Meshing

A uniform hexahedral mesh consisting ~8x104 cells per tube was generated using ANSYS 16 Meshing, as shown in Figure 5. The grid has two special characteristics: 1) 2 elements were used along the thickness of the tube to account for the conductive heat transfer and 2) a single inflation layer was used to model the near-wall region of the tube and fluid. The reasoning behind these two choices is the next subsection.

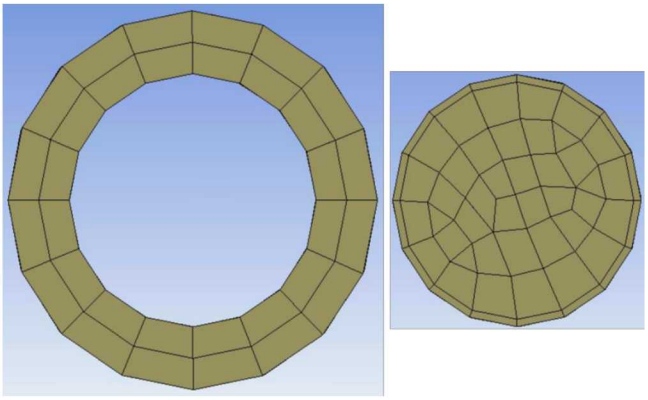

Figure 5.Left: Mesh used in a single tube used for all the tubes in the receivers. Right: Interior mesh fluid region requires a layer which is capable of yielding the Y+ value requirement.

3.2. Fluid Flow Modeling

The two receiver configurations shown in **Error! Reference source not found.** Figure 7 exemplify the two flow configurations that were chosen to be analyzed using pressurized air as fluid. The air flow was treated as a compressible flow. To reduce the domain size, the geometries were simplified for the flow models by removing the manifolds and using an equivalent recirculation boundary condition. Nonetheless, a flow distribution effectiveness study was performed in order to assure that the fluid flow was uniformly distributed in the manifolds, and the findings are discussed in the results section.

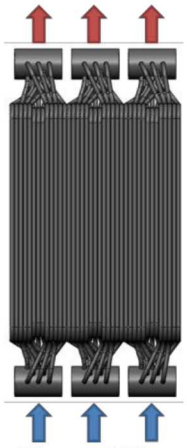

Figure 6.Flat Panel Receiver

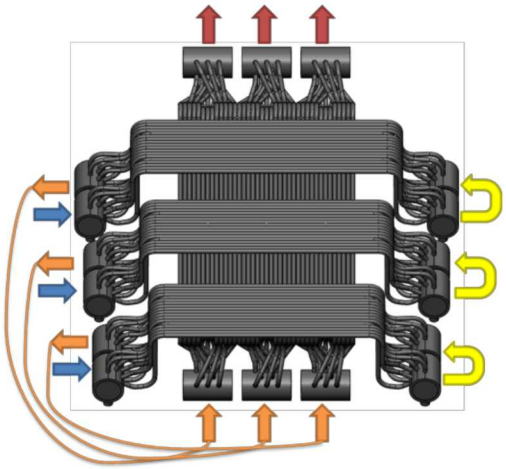

Figure 7.Bladed Panel Receiver

The SST k-ω turbulence model is used to solve for the turbulent flow inside the tubes. The model is more accurate and reliable for a wider class of flows because the wall boundary conditions for the k equation in the k-ω models are treated in the same way as the k equation is treated when enhanced wall treatments are used with the k- ε models [6]. This means that all boundary conditions for wall-function (coarse) meshes will correspond to the wall function approach. Since the range of $30 \leq Y+ \leq 300$ is so extensive, a single element inflation layer can be used as long as the Y+ value is still inside the range [6].

3.3. Conjugate Heat Transfer Modeling

A gray-body model was implemented to approximate the radiative losses between the tubes and the environment. The outer walls of the tube were assumed to have a constant emissivity of 0.8 and reflectivity of 0.1, assuming oxidized Inconel. The model considers the radiative interaction between the tubes to be negligible. Two-elements on wall were sufficient to yield grid independence for thermal conduction. The inner surfaces of the tubes were assumed to have a constant emissivity of 0.8 as well. The convective losses only considered natural convection, by assuming a constant heat transfer coefficient of 10-20 W/m^2-K at ambient conditions calculated based on the average wall temperature. The heat flux distribution profile obtained from the ray tracing studies output was applied as a heat generation profile boundary condition on the heated walls of the tube [6]. This enables the coupling of mixed thermal losses boundary condition with the internal domains consisting of tube thickness and fluid volume containing pressurized air.

4. BLADED RECEIVER TESTING

Two receivers were tested at the 220 ft. level (120 feet above ground level) of the solar tower at the National Solar Thermal Test Facility (NSTTF). The flat panel receiver, composed of 3 back panels shown in Figure 6, was the baseline receiver case as it is typical of receiver panel arrangements in existing CSP plants. The bladed panel receiver, ccomposed of 3 back panels and 6 blade panels shown in Figure 7, consisted of the flat panel receiver, but also included “blades” arranged at a 50° angle from vertical to enhance the light-trapping of the incoming irradiation from the heliostat field [5].

The flat panel receiver was tested on-sun on 09/09/2016. After this test, the rig was modified to hold the bladed panels in place and was tested on 09/19/2016. The results are evaluated in this section.

4.1. Testing conditions

The test loop designed (Figure 8) provided compressed air to the receivers at 800kPa and ~0.1 kg/s with associated sensors to measure temperature, mass flow rate, and pressure. The system used air as a heat transfer medium that was provided by an oil-free compressor at the ground level of the Solar Tower. An oil-free compressed air was used to ensure that the receiver tubes could be used again with a different heat transfer medium without being contaminated by oil in the lines. A 1,000 gallon air receiver tank was used in-line after the compressor to reduce the load/unloading cycles needed to keep a relatively constant pressure in the system (Figure 9).

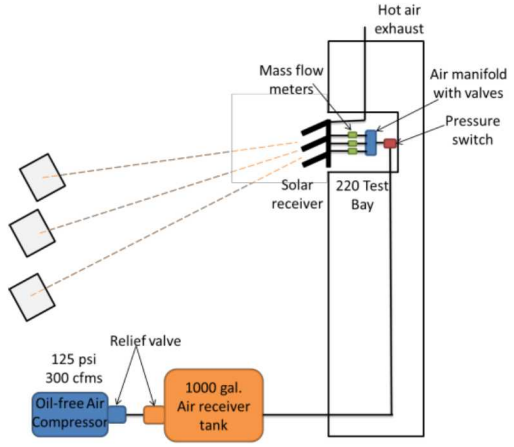

Figure 8.Simple schematic of the test loop for the flat panel and bladed receiver tests

Figure 9.Air compressor (right in image) and 1000 gallon air receiver tank (yellow tank in image)

The air flow is then separated in three sections as shown in Figure 10. Each flow loop had a temperature, mass flow rate, and pressure reading at the inlet. If there were transitions between panels (such as the bladed receiver) there were temperature measurements between these transitions. Temperature and pressure were measured at the outlet of the receivers (Figure 10Figure 11). Test and safety procedures are explained in detailed in by Ho et al. [9].

Figure 10.Alicat mass flow rate sensors attached to the three outlet manifold tank

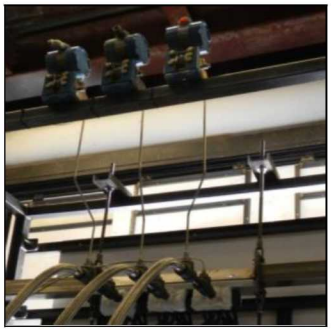

Figure 11.Three Rosemount pressure transmitters attached to the outlet receiver manifolds

4.2. Panel pre-oxidation

Inconel 625 sample coupons were oxidized and their reflectivity was measured. The oxidation was done at 800°C for different times as shown in Table 5. The last measurement was done on the flat caps of the panels oxidized. The goal was to oxidize the panels until an intrinsic solar reflectance was ~0.1. Figure 12 shows the comparison between oxidized and pristine samples.

Table 5.Reflectivity measurements of Inconel 625 oxidized samples.

Sample Oxidation			
Sample	Temperature (°C)	Time (hrs.)	Reflectivity
1	-	-	0.519 ± 0.007
2	800	1	0.208 ± 0.006
3	800	5	0.18 ± 0.001
4	800	24	0.151 ± 0.001
Panel	800	30	0.124 ± 0.004

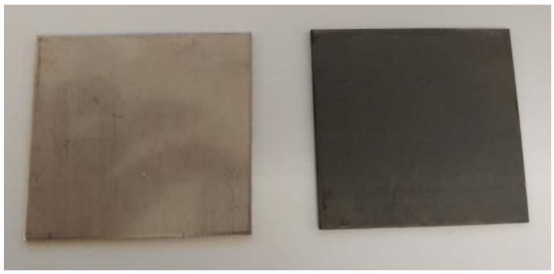

Figure 12.Sample 1 and Sample 4 from

4.3. Leading tube failure prevention

The leading edge/tube of the bladed receiver panels is subject to very high solar fluxes relative to the rest of the tubes due to higher view factors. Optical modeling showed the potential for overheating due to the heat flux being up to 3.5 times higher than the rest of the tubes on the bladed panel. Figure 13 shows the leading edge painted with high temperature white paint. After the paint cured, the solar reflectivity was measured to be 0.54.

Figure 13.Bladed receiver panels with front tube painted white with VHT Flame Proof Header Paint.

4.4. Receiver support structure, spillage board and insulation

The receiver required a support structure that could accommodate the two receiver designs to be tested. The structure was required to hold the weight of the panels, the spillage board required for on-sun testing, and thermal insulation for all plumbing. This structure was arranged on two sliding rails to be able to move the structure back and forth in the test bay.

Figure 14 shows the final test structure for the bladed panel receiver test. The spillage boards have been installed on the front of the receiver protecting the structure from incident flux. Figure 14 also shows the thermal insulation installed behind the flat panel receiver. The insulation covered the inlet and outlet headers as well as the back of the receiver tubes to prevent heat loss from the system. Any hose that had air going into a receiver panel was insulated.

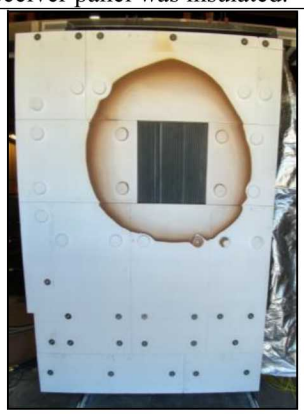

Flat panel receiver in place after on-sun testing.

Bladed receiver in place after on-sun testing.

Thermal insulation in place for the flat panel receiver tests (view is behind the receiver at the plumbing)

Thermal insulation in place for the bladed receiver tests (view is behind the receiver at the plumbing)

Figure 14.Spillage and insulation around the receiver mounted in the support structure. The brown color is from the bond burning out on the spillage board.

5. TEST AND MODEL RESULTS

The variation in all the temperatures recorded by the thermocouples was used to determine the steady-state regions where the relative uncertainty of the temperature increase was below 2%. The temperature increase was recorded throughout all the tests and the average of the temperatures and standard deviations were used to estimate the overall error propagation. The impact on the mass flow rate fluctuation and the heat flux centering were included in the error propagation analysis. In depth details were published by Ho et al. [9].

In order to compare the flat and bladed receivers, all the results were done as a function of the average irradiance. The average irradiance was determined by dividing the incident power over the entire exposed area.

5.1. Pressure drop

Although the pressure drops across the receivers are below 10% for both receivers, the comparisons were made to understand how to improve the computational models. The only difference identified between the tests and the models which could have an impact on the lower pressure drop exhibited on the models, is that the surface roughness value is the one for pristine Inconel 625 (25 μm) [6] as opposed to the value of an oxidized surface. Unfortunately the roughness could not be determined since it was not part of the scope of the project. Figure 17**Figure 18** show the comparison of the pressure drop recorded during the tests and the pressure estimated in the models.

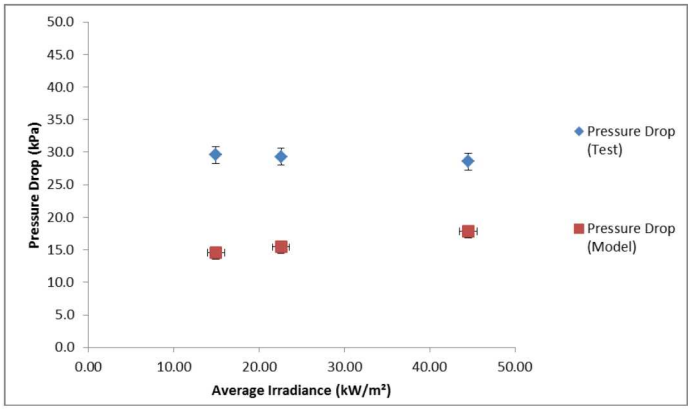

Figure 15.The pressure drop comparison on the flat receiver as a function of the average irradiance incident on the receiver [9].

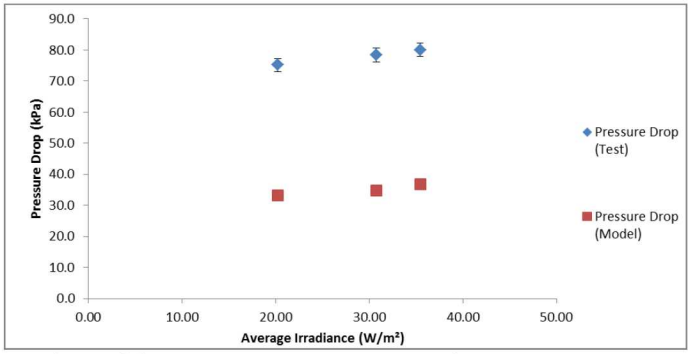

Figure 16.The pressure drop comparison on the bladed receiver as a function of the average irradiance incident on the receiver [9].

5.2. Temperature increase

The temperature rises recorded during the tests of both receivers are lower than those computed by the models. This could be mainly caused by the models not considering forced convective losses. Only estimates of the heat transfer coefficient on the surface of the receivers could be used by the assuming average wind speeds instead of wind gusts. Figure 17Figure **18** show the graphical comparisons of the temperature rise in the pressurized air flowing through the receiver.

Figure 19Figure 20 show the comparison of the surface temperature. The location of the thermocouple in the back of the receiver is 20 cm from the top from the exposed tube length. This reference temperature was used to track the peak temperatures. The models showed that the peak temperature was between 60-100°C higher, in average. Therefore it served as a good monitor to avoid any damage on the receiver. The temperatures recorded during the tests of both receivers are lower than those computed by the models. This is mainly caused by the models not considering forced convective losses as well as variations on the intrinsic absorptance of the surface.

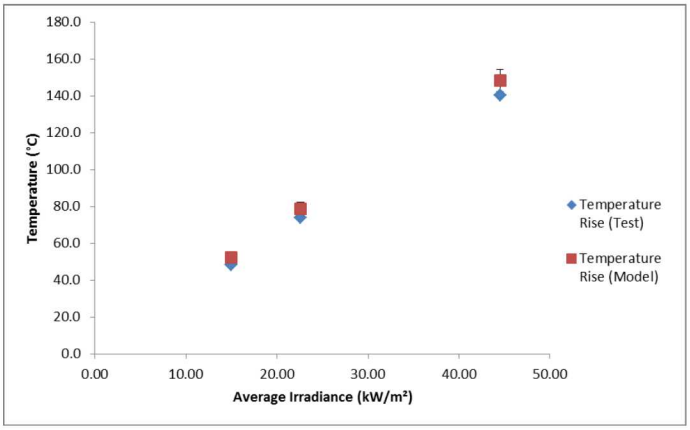

Figure 17.Temperature rise of pressurized air through Flat receiver as a function of the incident average irradiance [9].

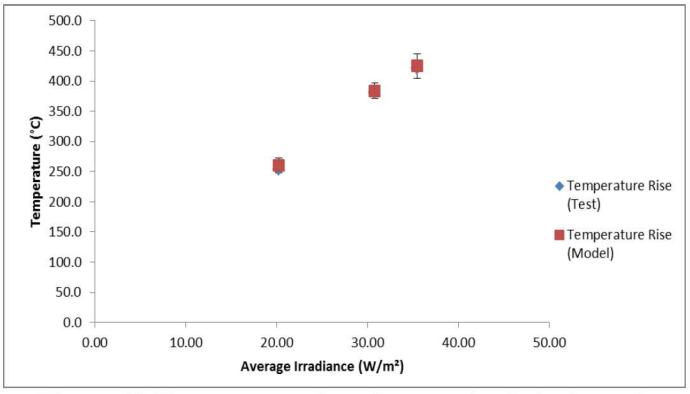

Figure 18.Temperature rise of pressurized air through Bladed receiver as a function of the incident average irradiance [9].

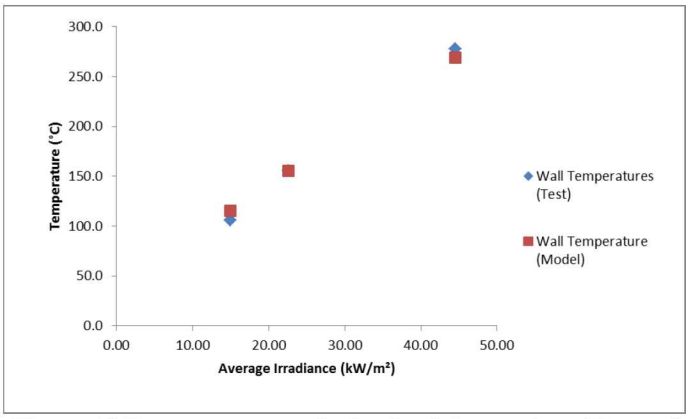

Figure 19.Temperature at the back of the receiver 20 cm of the top from the flat receiver as a function of the incident average irradiance [9].

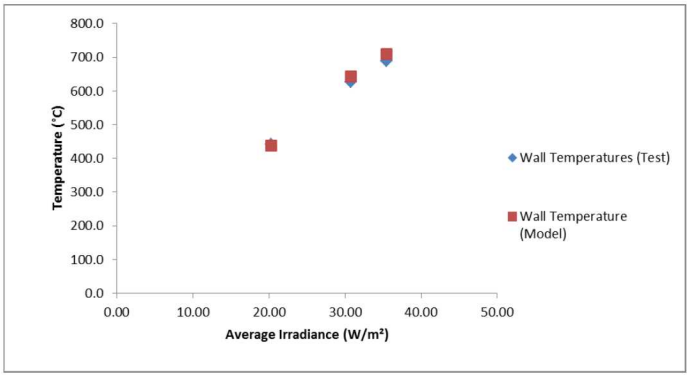

Figure 20. Temperature at the back of the receiver 20 cm of the top from the bladed receiver as a function of the incident average irradiance [9].

5.3. Receiver thermal efficiency

The data collected in the steady-state region was used to compute the thermal efficiencies as a function of the power incident on each receiver. Figure 21 shows the thermal efficiencies using the formula:

$$Thermal\ Efficiecncy = \frac{\sum \dot{m} \int_{Tin}^{Tout} C_p(T)dT}{\dot{Q}_{incident}}$$

where $\dot{m}$ is the total mass flow rate of air per section, Tin and $Tout$ are the Inlet and outlet air temperatures, $C_p(T)$ is the heat capacity of air and $\dot{Q}_{incident}$ is the total power incident on the receiver.

The thermal efficiencies obtained from the tests of both receivers are compared to the efficiencies estimated from the models. It can be inferred that since the temperatures are higher in the models, the modeled receiver efficiencies are higher than those in the tests. Nonetheless, the bladed receiver trend observed in Figure 21 shows positive results which show an enhancement of thermal efficiency over the flat receiver [9].

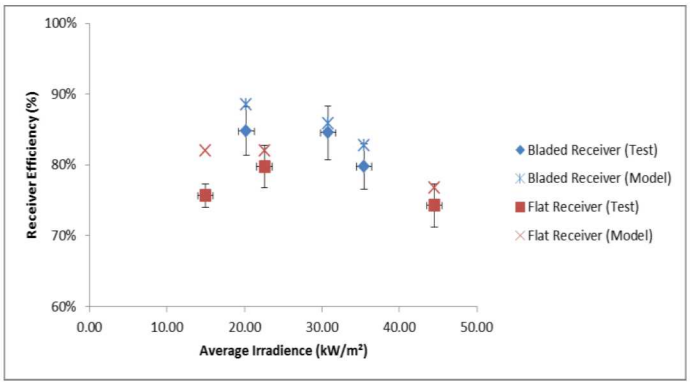

Figure 21.Thermal efficiency comparison between the model predictions and the test results [9].

6. CONCLUSIONS AND FUTURE WORK

Fractal-like receiver designs with novel light-trapping geometries and features have been developed and tested. The bladed panel receiver configurations were simulated and shown to reduce radiative heat losses and increase thermal efficiencies by increasing the effective solar absorptance and reducing heat losses [9].

Macro-scale tests were conducted using flat and horizontal bladed receiver designs. Pressurized air was used as the heat-transfer fluid. The irradiance on the tubular receiver panels was prescribed to yield similar average irradiance values for the two sets of tests, which ranged from ~20 – 70 kW/m^2. The peak flux on the aperture of the bladed receiver panel (over 200 kW/m^2) was significantly higher than the peak flux on the flat panel (over 80 kW/m^2). This is one of the advantages of the fractal-like designs, the ability to accommodate higher concentration ratios with smaller optical apertures [9]. Results showed that the air temperature rise in the bladed receiver panel was 200 – 300 °C higher than in the flat panel while the thermal efficiencies were ~5 percentage points higher [9].

Currently, the plan for the near future is to develop a test-loop using pressurized gas bottles to test the receiver performance at high pressure and temperature while investigating the effectiveness of different gases and mixtures as heat transfer media.

7. AKNOWLEDGMENTS

Sandia National Laboratories is a multi-program laboratory managed and operated by Sandia Corporation, a wholly owned subsidiary of Lockheed Martin Corporation, for the U.S. Department of Energy's National Nuclear Security Administration under contract DE-AC04-94AL85000. The United States Government retains and the publisher, by accepting the article for publication, acknowledges that the United States Government retains a non-exclusive, paid-up, irrevocable, world-wide license to publish or reproduce the published form of this manuscript, or allow others to do so, for United States Government purposes.

8. REFERENCES

[1] Pacheco, J. E., 2002, "Final Test and Evaluation Results from the Solar Two Project," SAND2002-0120, Sandia National Laboratories.

[2] U.S.Department of Energy, 2011, "SunShot Initiative."

[3] Friefield, J. M., and Friedman, J., 1974, "Technical Report No. 1: Solar Thermal Power Systems Baded on Optical Transmission,"Rocketdyne Division, Rockwell International.

[4] "U.S. Patent Application 14535100, Filed Nov. 6, 2014, BLADED SOLAR THERMAL RECEIVERS FOR CONCENTRATING SOLAR POWER."

[5] Christian, J., Ortega, J., Ho, C., Yellowhair, J., 2016, "Design and modeling of light-trapping tubular receiver panels," ASME 2016 Energy Sustainability and Fuel Cell Conference, Charlotte, NC.

[6] Ortega, J., Khivsara, S., Christian, J., Ho, C., Yellowhair, J., Dutta, P., "Coupled Modeling of a Directly Heated Tubular Solar Receiver for Supercritical Carbon Dioxide Brayton Cycle: Optical and Thermal-Fluid Evaluation", Applied Thermal Engineering, Volume 109, Part B, 25 October 2016, Pages 970–978

[7] Ortega, J., Khivsara, S., Christian, J., Ho, C., Dutta, P., "Coupled Modeling of a Directly Heated Tubular Solar Receiver for Supercritical Carbon Dioxide Brayton Cycle: Structural and Creep-Fatigue Evaluation", Applied Thermal Engineering, Volume 109, Part B, 25 October 2016, Pages 979–987

[8] ASME Boiler and Pressure Vessel Code. New York, NY: American Society of Mechanical Engineers, 2013

[9] Ho, C., Ortega, J., Christian, J., Yellowhair, J., 2016, "Fractal-Like Materials Design with Optimized Radiative Properties for High-Efficiency Solar Energy Conversion," SAND2016-9526, Sandia National Laboratories.